

## **Gabor deconvolution applied to a Blackfoot dataset**

Victor Iliescu and Gary F. Margrave

### **ABSTRACT**

A new deconvolution technique was applied to the data gathered over the Blackfoot field owned by PanCanadian Petroleum Ltd. In this paper, the Gabor method for deconvolution, which is a nonstationary, transform-based technique is compared with the familiar spiking deconvolution, which is operator based. The Gabor method compensates for the time-variant frequency attenuation, which is the main cause of the nonstationarity of seismic signals. The nonstationary Gabor deconvolution is a robust and flexible method that successfully replaces the stationary, classical Wiener deconvolution. This paper shows, using real data examples, that the Gabor method can be applied with confidence as an alternative to the Wiener deconvolution and the time-variant spectral whitening (TVSW) techniques. Within the design gate of Wiener deconvolution, Gabor deconvolution produces similar results. Outside this gate, Gabor deconvolution is superior.

### **INTRODUCTION**

This paper compares, from an interpretation point of view, the results of two different types of deconvolution applied to seismic data in two processing flows. The methods are stationary Wiener deconvolution followed by the time-variant spectral whitening (TVSW) technique of the stacked section, and Gabor deconvolution. Gabor deconvolution was applied before stacking to the raw data, and again after stack, replacing the TVSW technique.

In the Gabor deconvolution case, either minimum-phase or zero-phase can be chosen while the TVSW technique is only a zero-phase process. Therefore, Gabor deconvolution was studied in both cases, with minimum-phase before stack and zero-phase after stack to produce a direct comparison with the spiking deconvolution and the TVSW techniques, and with minimum-phase before and after stack, assuming that the data is minimum-phase.

The Gabor transform uses a Gaussian function to achieve temporal localization. Multiplying the signal by a window function  $g(t-\tau)$ , a Gaussian, centred at time  $\tau$ , results in a modified signal that is a function of two times, the fixed time,  $\tau$  and the running time  $t$ . A suite of localized traces are generated by repeating this operation as the analysis function is translated along the signal. If at every fixed time,  $\tau$ , a Fourier transform is applied, the result is a time-frequency decomposition. Deconvolution can be conducted in this 2-D (time-frequency) plane in a similar manner as the 1-D frequency domain deconvolution, thus finding the deconvolution operator by smoothing the magnitude of the Gabor spectrum of the signal. (See Margrave and Lamoureux, 2001, for a complete discussion.)

## DATA ANALYSIS

### Acquisition parameters and a brief geological description

The Blackfoot field is located in Township 23, Range 23, West of the 4<sup>th</sup> Meridian, near Strathmore, Alberta. The line processed was recorded in 1997 and is oriented east to west in the Blackfoot field. From the three components recorded (3-C geophones), the 10 Hz, vertical component was used to test the Gabor deconvolution because it represents the industry standard. Receiver interval was 20 m. There were 151 receiver stations in total and the stacking fold is about 159 in the middle of the line. The exploration objective of this line was to image the incised paleo-valleys within the Glauconite formation of the Lower Cretaceous Mannville Group. The Glauconitic sandstones vary from zero to 40 m in thickness and are found in structural and stratigraphic traps. Reservoir rocks are subdivided in this area into three units corresponding to three phases of incision (Figure 1): Lower Channel, Lithic Channel, and Upper Channel. According to Miller et al. (1995), all three units may not be present everywhere. On the seismic displays in this paper, the incised channels appear between the CDP's 350 to 450, in the time window from 1.05 to 1.1 seconds.

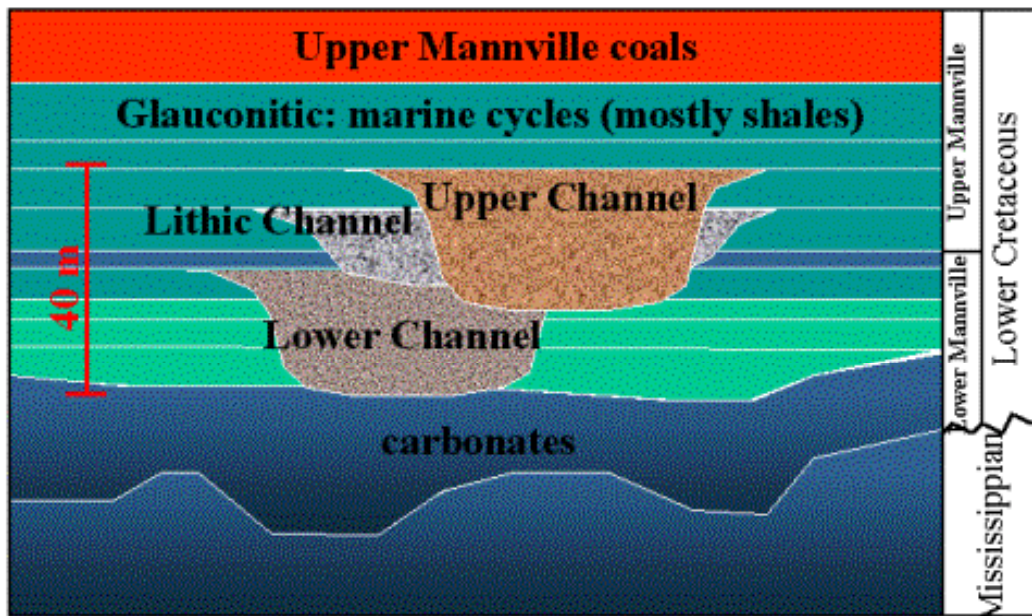


FIG. 1. Blackfoot Geology.

### Gabor deconvolution parameters

A more detailed discussion of these parameters may be found in Henley and Margrave (2001). Here, we will give a brief description of the Gabor deconvolution parameters used in the processing flow.

The width of the analysis window is an important parameter in the sense that a wide analysis window will have excellent resolution in frequency but poor temporal resolution; conversely, a short analysis window will have greater time resolution but

poor frequency resolution. There is little physical justification in using a window narrower than the length of the embedded wavelet, which is presumed to be between 0.1-0.4 seconds in length. In this study, the length of the Gaussian window was chosen to be 0.4 seconds. Other possibilities were not examined.

Another important parameter is the time increment between analysis windows. This parameter controls the redundancy of the Gabor spectrum and directly influences the computation time. It also determines the minimum possible time scale on which the algorithm can adapt. This parameter depends on the window width described above and it should usually set to be less than the window width. In this study, the time increment was set at 0.04 seconds.

A third parameter used in the Gabor deconvolution is the method of spectral estimation, which can be a straightforward discrete Fourier transform (DFT) or the Burg spectrum (Claerbout, 1976) of the windowed signal. In the case of the Burg algorithm, the number of the prediction-filter coefficients used in calculating the Burg spectrum is inversely proportional to the smoothness of the resulting spectral estimate. For example, a small coefficient number is similar to using the Fourier estimation and applying stronger smoothing. In the processing flow, six coefficients were used for the deconvolution of the raw data and twelve for whitening the stacked data.

The fourth parameter controls the phase of the deconvolution operator, which can be zero-phase or minimum-phase. Both of these options were tested. Assuming that the data is minimum-phase, the minimum-phase option is to be preferred to zero-phase. This was the first option for the Gabor deconvolution applied before and after stack. To be consistent with the parallel flow using the Wiener deconvolution, a second product was computed using minimum-phase deconvolution before stack and the zero-phase deconvolution (equivalent to the TVSW technique) after stack.

The deconvolution operator can be derived from the magnitude (linear) Gabor spectrum or from the logarithmic Gabor spectrum of the data. Both choices were examined and the magnitude spectrum was used because it resulted in a stronger whitening of the data.

The number of passes of the smoothing operator is a parameter which determines how many times the smoother is applied to the Gabor spectrum for wavelet estimation. This parameter was set to unity for the Fourier and Burg method in the Gabor deconvolution applied before stack and sixteen for the second application, after stacking. The smoother geometry is a boxcar, but applying it many times is similar to smoothing with a very large Gaussian. (This is a consequence of the central limit theorem; Claerbout, 1992.)

The frequency dimension of the smoothing window determines the number of the points to be smoothed along the frequency axis. This parameter was set to 21 Hz first pass in the flow and 16 Hz in the second, after stacking. The frequency dimension controls the temporal size of the assumed wavelet estimate. Shorter wavelets have smoother spectra.

The time dimension of the smoothing operator determines the number of spectral magnitude points to be smoothed in time. This parameter was set to 0.8 seconds in the first pass in the flow, and 0.5 seconds in the post-stack process. This parameter controls the nonstationarity of the deconvolution. The longer this value, the more stationary the deconvolution becomes.

The stability factor is similar to adding white noise as in stationary deconvolution, to prevent any division by zero. The value was set to 0.0001.

### **Spiking deconvolution & TVSW parameters**

In the case of Wiener spiking deconvolution, some parameter testing was done and the parameters with the best results have been established. A detailed description of these parameters can be found in Yilmaz (1987) and the Help of the ProMAX processing software.

The type of deconvolution was minimum-phase spiking with a deconvolution operator length of 0.24 seconds. The Wiener design gate was set between 700 and 1900 milliseconds. The white noise level was set to 0.001.

For the TVSW technique the spectral-balancing scalar length was 1 second and 12 filter panels have been used. The lowest frequency whitened was 10 Hz and the highest was 100 Hz. See Yilmaz (1987) for a description of this method.

### **Processing flows**

Two processing sequences have been used in parallel to test Gabor deconvolution and to compare it with the familiar Wiener deconvolution. In the case of Wiener spiking deconvolution the flow is shown in Figure 2. The Gabor deconvolution processing flow is shown in Figure 3. Comparing these two processing sequences a number of differences become evident. In the case of Gabor deconvolution the exponential gain correction was omitted from the flow because the nonstationary nature of the process causes it to boost the amplitudes.

The residual statics and the velocity analysis were done in the Wiener deconvolution flow and applied to Gabor flow in order to have the same comparison parameters.

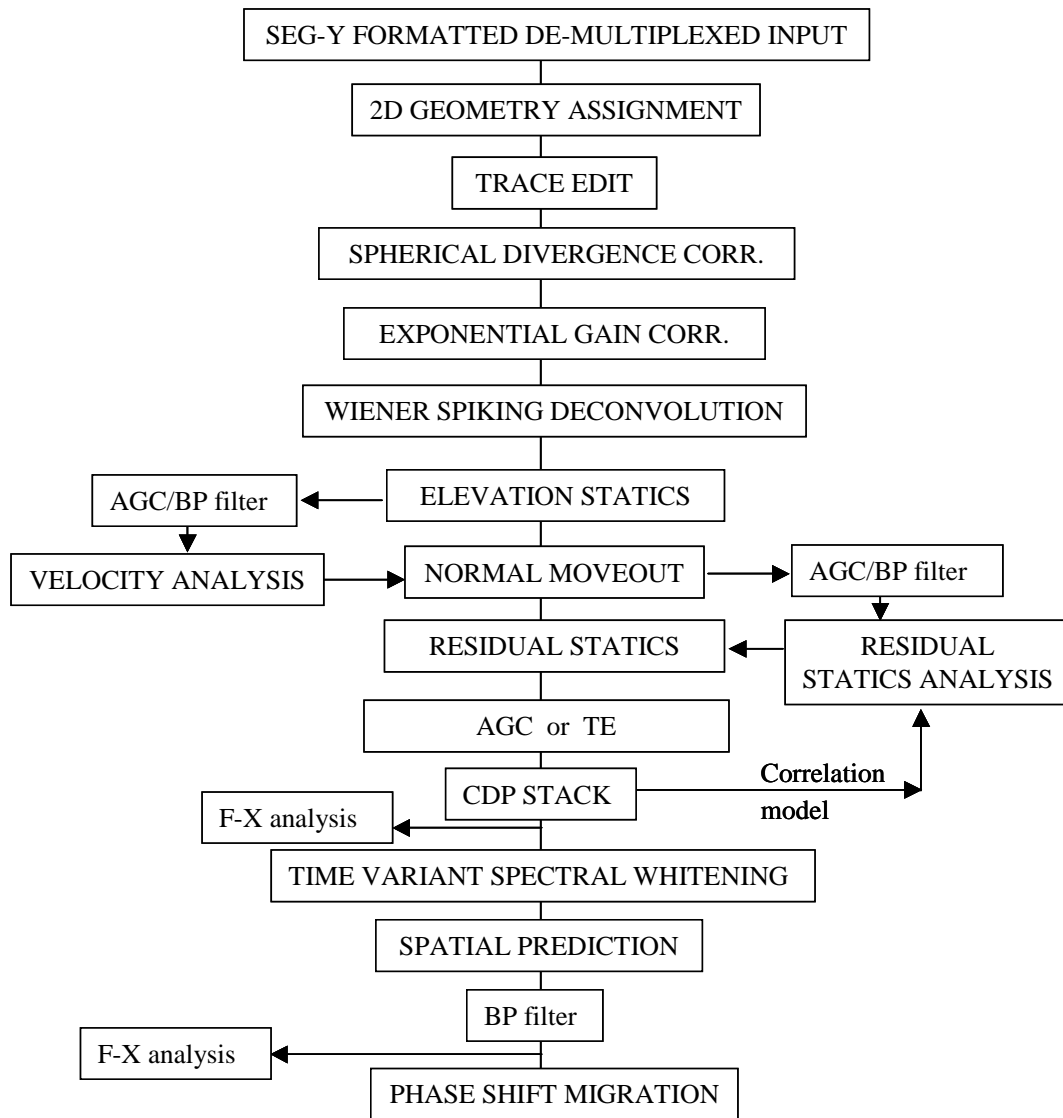


FIG. 2. The processing flow of the Wiener spiking deconvolution. The result of this flow is the Wiener/TVSW section.

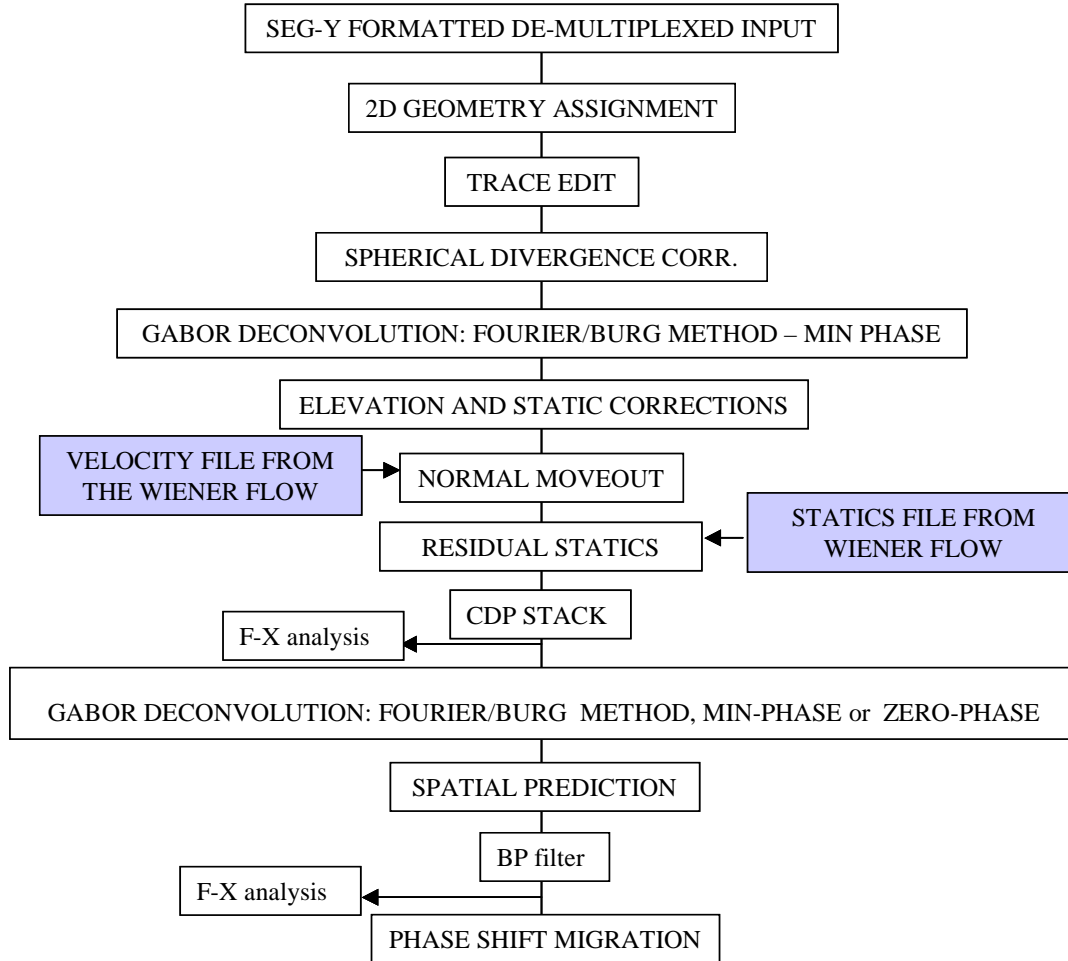


FIG. 3. The processing flow of the Gabor deconvolution sections. Two final sections have been generated by this flow, Gabor/Fourier section and Gabor/Burg section.

## DISCUSSION

A typical shot record is shown in Figure 4. The result of the Gabor deconvolution (Burg method) applied to the data after geometry assignment and editing, can be observed in Figure 5 while in Figure 6 the same shot record after Wiener deconvolution is displayed. Before Wiener deconvolution, exponential gain correction was applied to the data while Gabor deconvolution performed without it (see Figures 2 and 3).

From these pictures we observe at least three significant differences. First, Wiener deconvolution has overwhitened the data above the deconvolution gate, set between 0.7 and 1.9 seconds. A strong reflection can be seen at approximately 0.3 seconds in Figure 5 (Gabor deconvolution) but there is nothing coherent in Figure 6 (Wiener deconvolution). The overwhitening is a side-effect, typical in stationary processes where the operator is designed within a gate and then is applied to the whole data, due to the differences in the spectral ratios in different temporal windows. Secondly, in the zone of interest (0.8-1.4 seconds), events on Gabor display seem to be tighter and

more compressed (better resolution). Thirdly, the ground roll has been better suppressed by Gabor deconvolution.

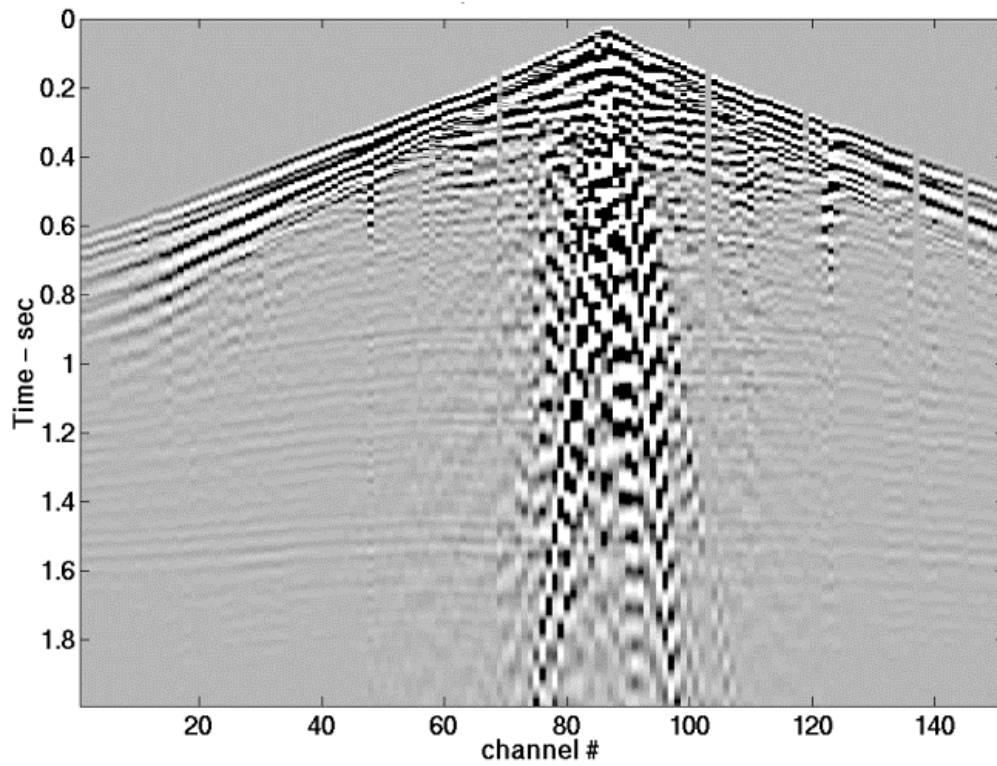


FIG. 4. Raw shot # 81.

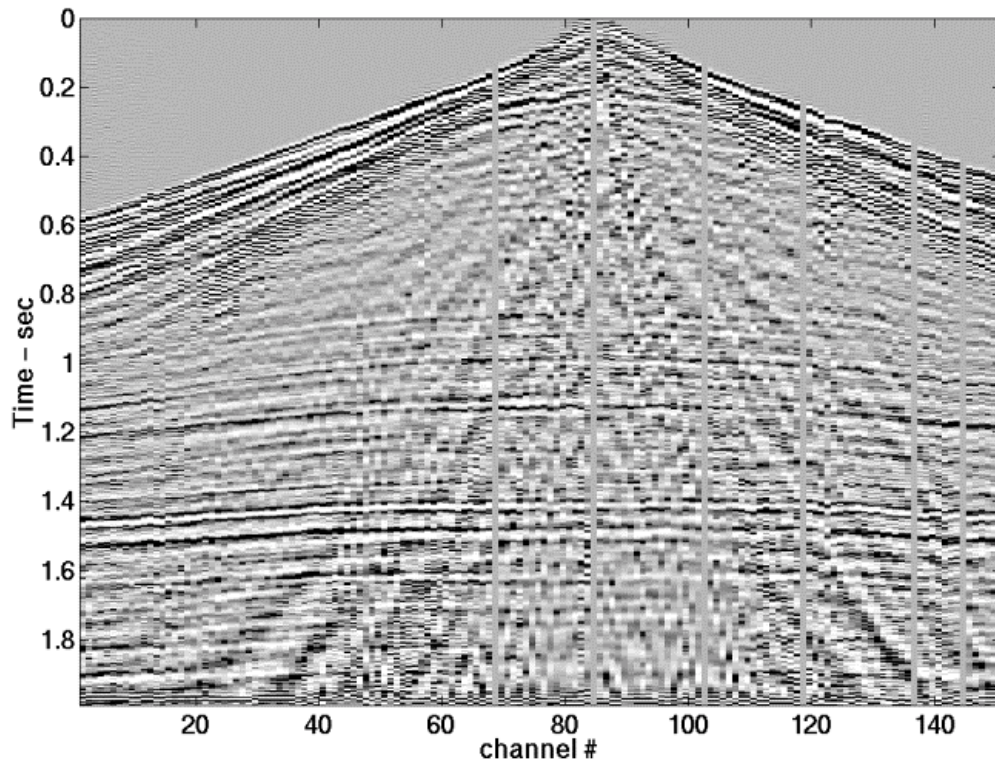


FIG. 5. Shot # 81 after Gabor/Burg deconvolution.

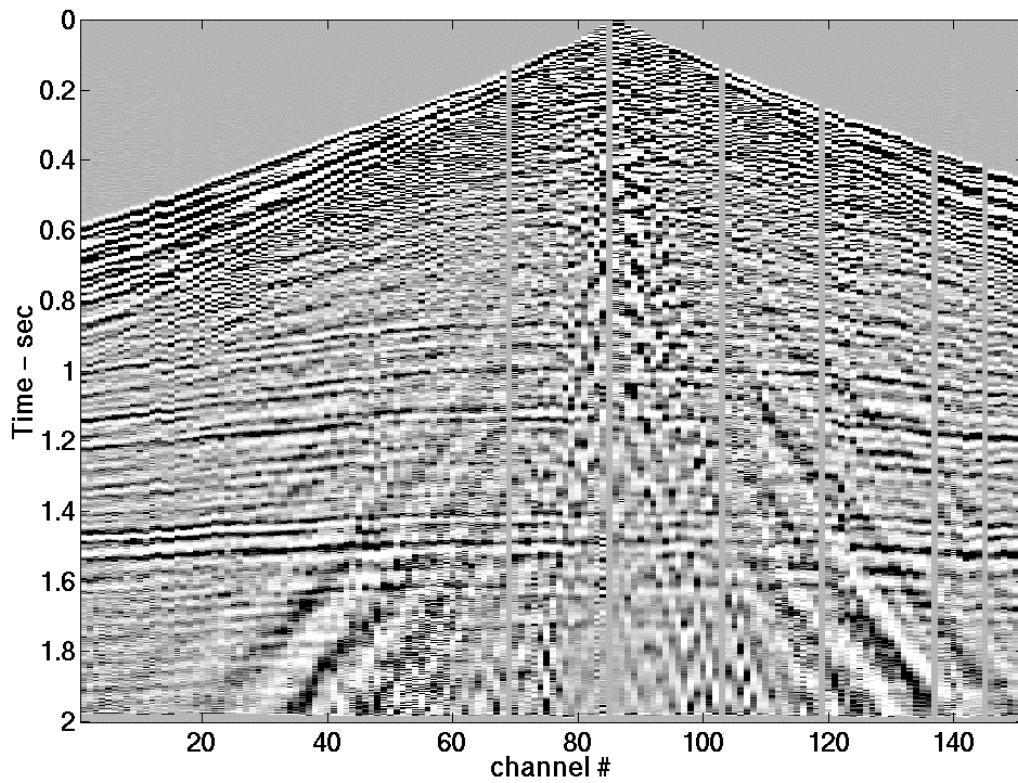


FIG. 6. Shot # 81 after Wiener deconvolution. Trace Equalization (0.8 – 1.6 seconds) applied for display purpose.

After deconvolution, elevation and static corrections were applied and a velocity analysis was conducted. Next, moveout corrections were applied using a set of preliminary velocity picks. Then residual statics corrections were calculated and applied. The velocity analysis was repeated to update the previous velocity picks and NMO corrections were applied again in an iterative process. This important sequence in the flow was performed on the output of the Wiener spiking deconvolution and same values for elevation statics and final velocity picks, as well as for the residual statics were applied to the Gabor deconvolution flow.

The next step in the processing flow was CDP stacking. Figure 7 shows the stacked section after Gabor/Fourier method and Figure 8, the Gabor/Burg method. In Figure 9a, the stack of the Wiener method with a prestack trace equalization (TE) is shown, while in Figure 9b a similar stack is shown but with a prestack AGC replacing the TE. The TE time gate was 0.8 – 1.6 seconds and the AGC length was 0.5 seconds. The AGC step from the Wiener flow was omitted in the Gabor sequence (compare Figures 2 and 3). In the Gabor nonstationary method, this additional adjustment is not needed because the Gabor operator automatically balances the trace. AGC was necessary in the stationary Wiener case to improve the efficiency of the stationary process.

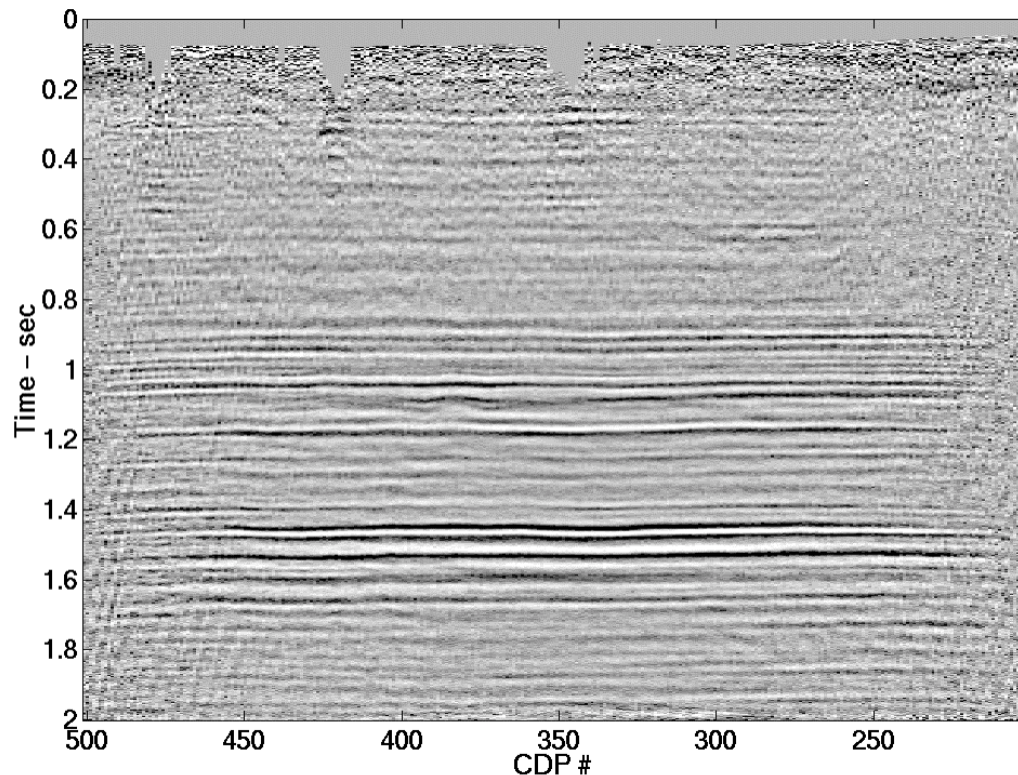


FIG. 7. Stack of the Gabor/Fourier deconvolution.

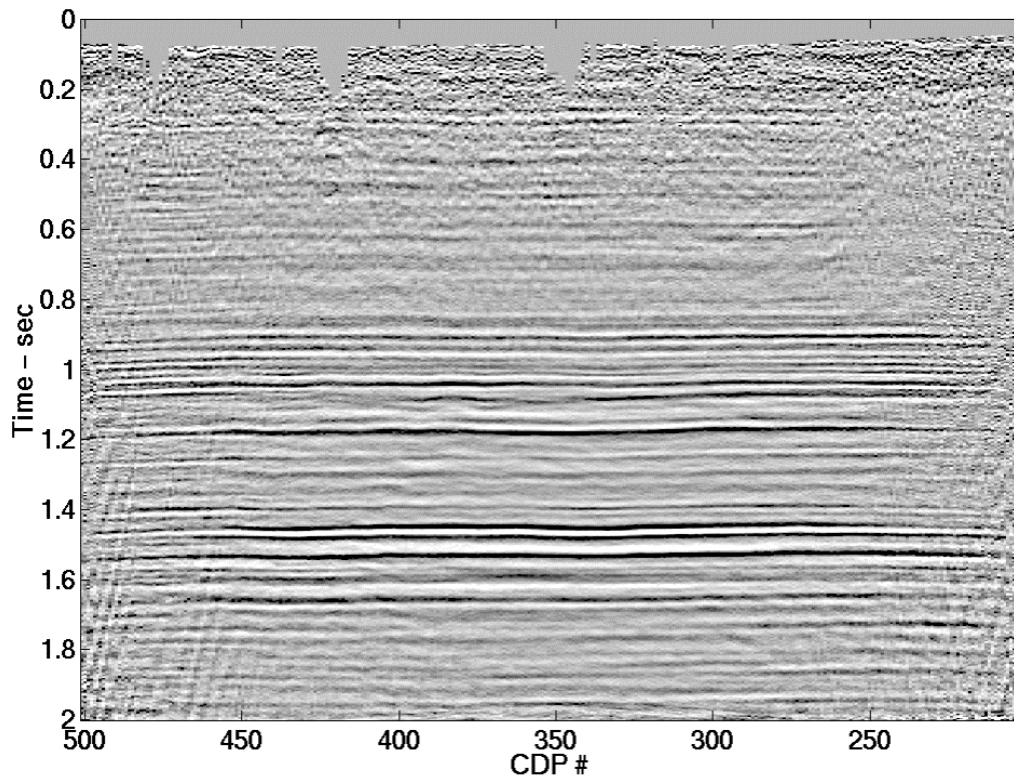


FIG. 8. Stack of the Gabor/Burg deconvolution.

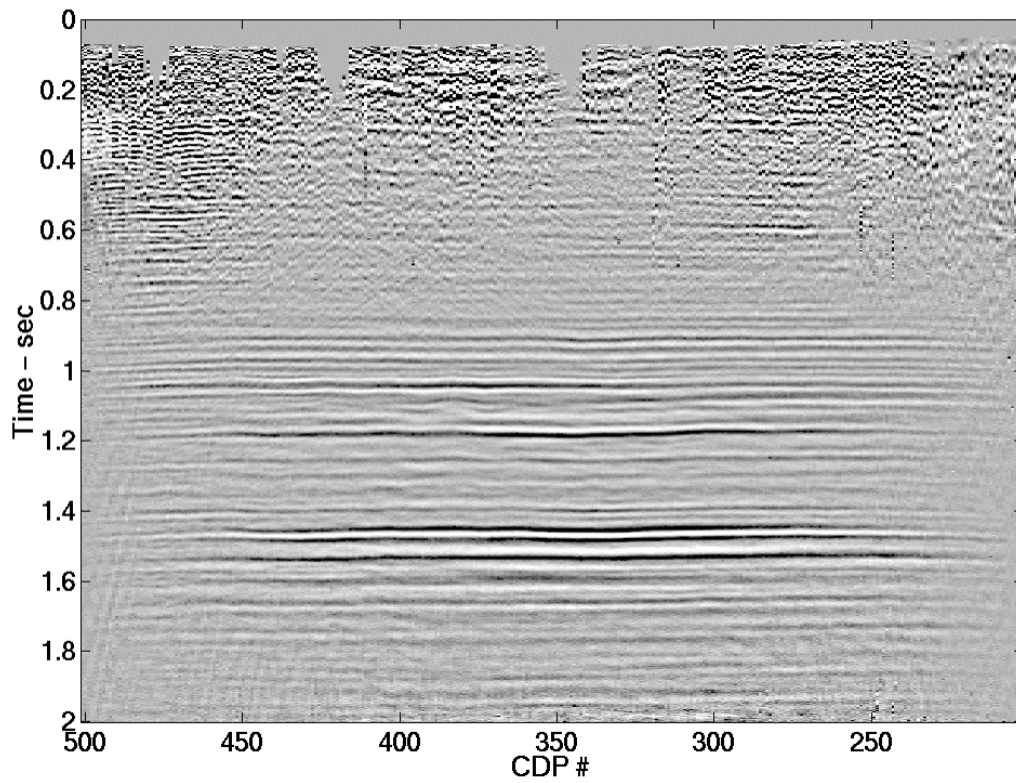


FIG. 9a. Stack after Wiener spiking deconvolution. TE applied for display purpose.

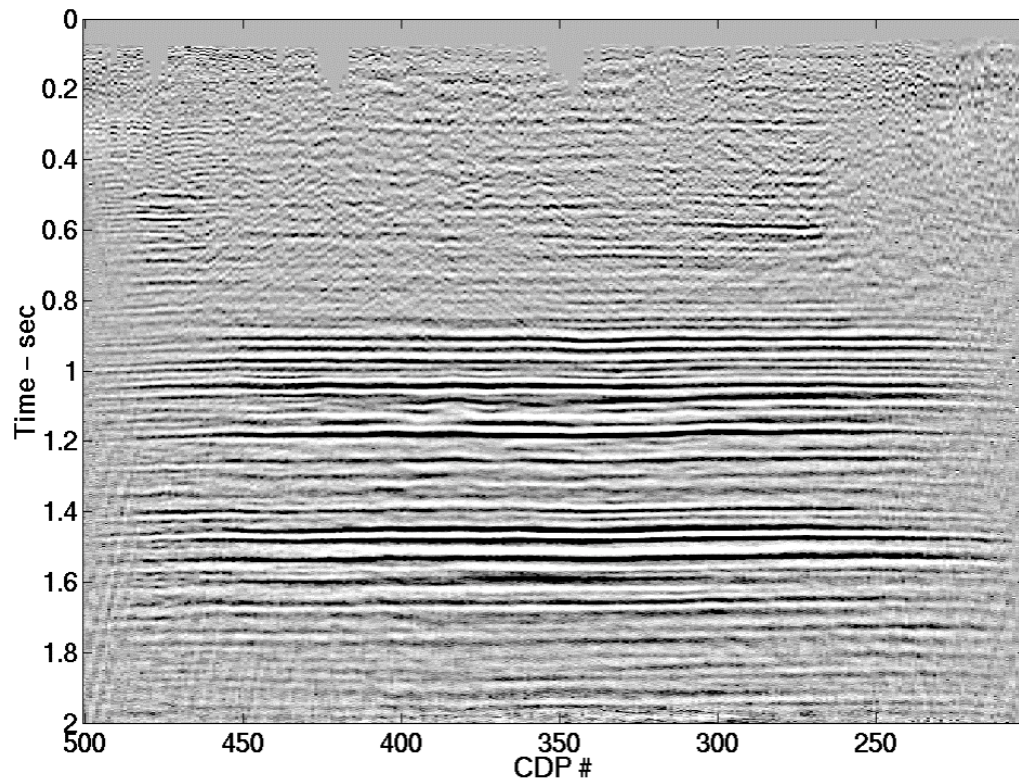


FIG. 9b. Brute stack after Wiener spiking deconvolution. AGC applied.

During the stacking process, the incoherent noise induced in data by the deconvolution process is suppressed so, these sections are presented with no bandpass filter applied. Stacking process alone acts as a signal enhancement by attenuating noise. Even an f-k filter was not necessary in this case because the deconvolution process did a very good job in suppressing the coherent noise trains (e.g. ground roll).

On all these sections, the Mississippian event can be observed at approximately 1050 seconds. The Glauconitic channels start to develop from the CDP 350 toward the left.

The F-X spectra of the stacked sections were also examined to observe the phase coherence of the record in all cases and to note the differences between the methods. In performing this test, a nominal temporal window was defined to span the zone of interest (0.6 – 1.3 seconds). The spectral continuity on these plots is a direct measure of the signal strength in the frequency domain (Margrave, 1999).

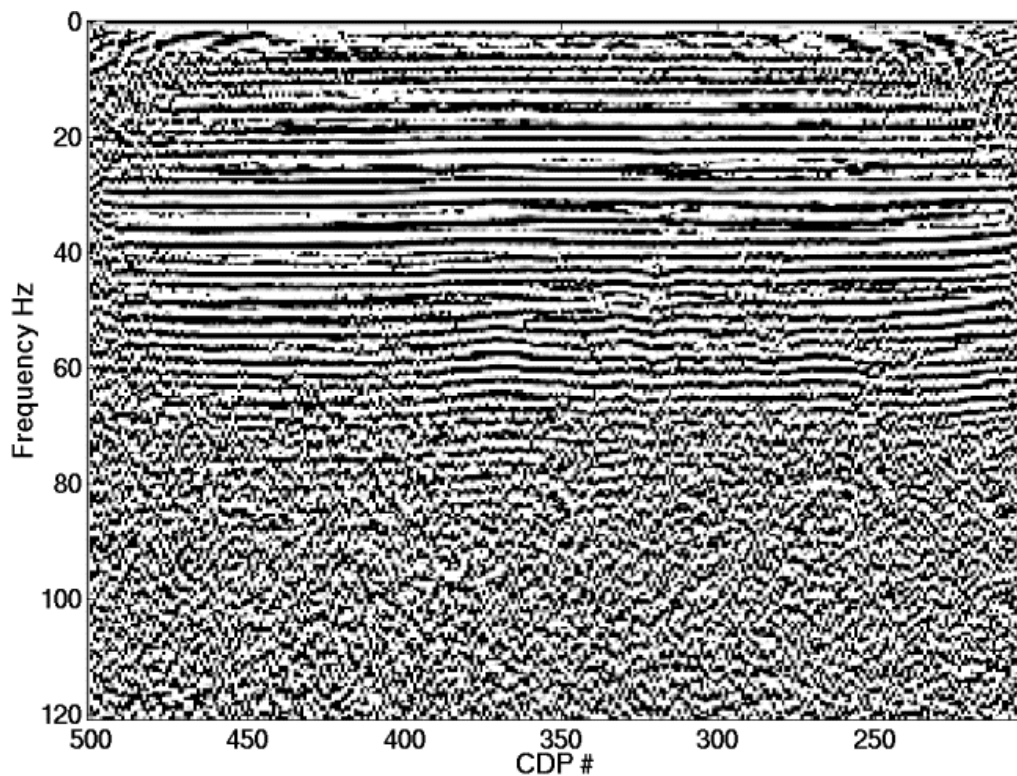


FIG. 10. F-X phase spectrum in the time window 0.6 – 1.3 seconds of the Gabor/Fourier stack section.

In Figures 10 and 11 are the F-X phase spectra for the zone of interval (0.6-1.3 sec.) after the Gabor deconvolution with the Fourier and Burg methods. In Figure 12 is the F-X phase spectrum from the Wiener spiking deconvolution section. In all cases phase coherence indicates signal up to 75 Hz. The Burg result seems to be slightly superior with packets of phase coherence near 85 Hz.

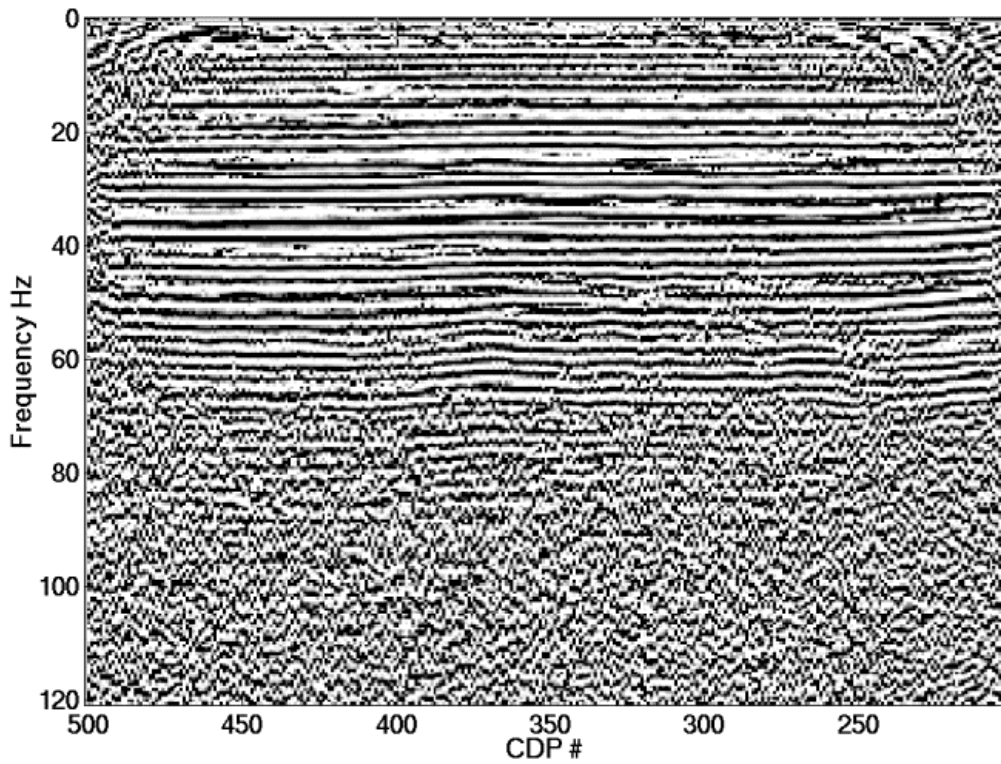


FIG. 11. F-X phase spectrum in the time window 0.6 – 1.3 seconds of the Gabor/ Burg stack section.

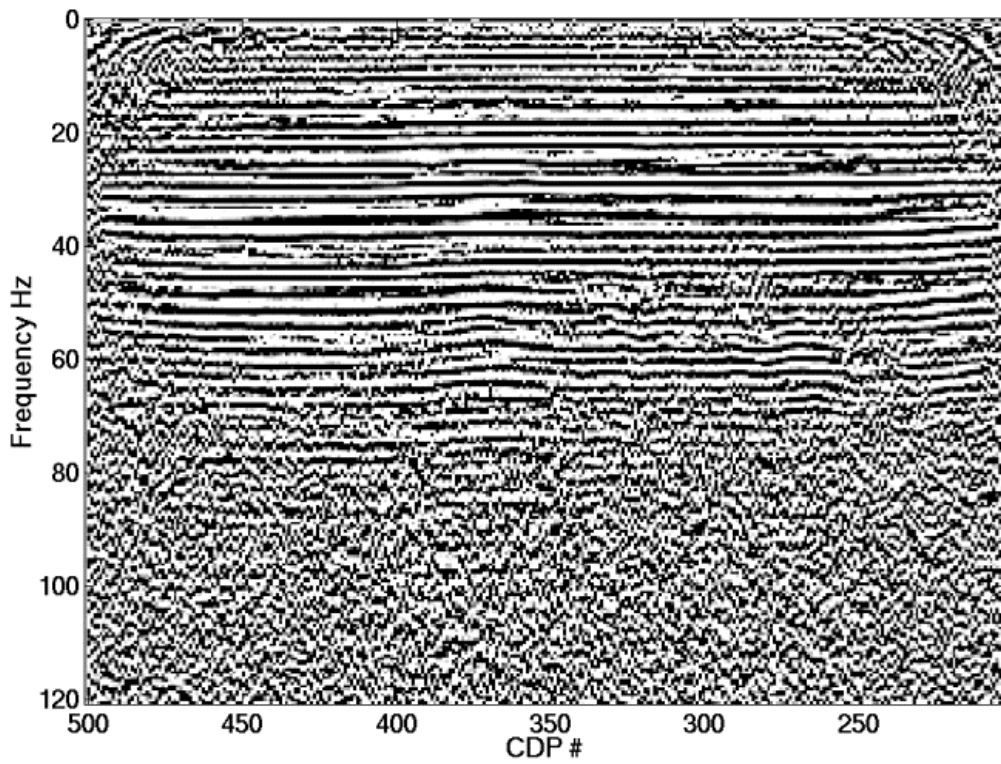


FIG. 12. F-X phase spectrum in the time window 0.6 – 1.3 seconds of the Wiener stack section.

The average values for the amplitude spectra were also analyzed in all the cases. In Figure 13, there are the representations of the mean amplitude spectra of all three sections calculated in the time window of 0.6-1.3 seconds. From this representation it can be observed that the mean amplitude spectra present similar characteristics in general. There is a better similarity between Gabor/Fourier and Wiener deconvolution, and in particular the Burg deconvolution stands out with greater magnitudes at frequencies greater than 50 Hz. Since these spectra were white before stack, the extent of de-whitening indicates the noise level. Conversely, greater spectral power suggests stronger signal.

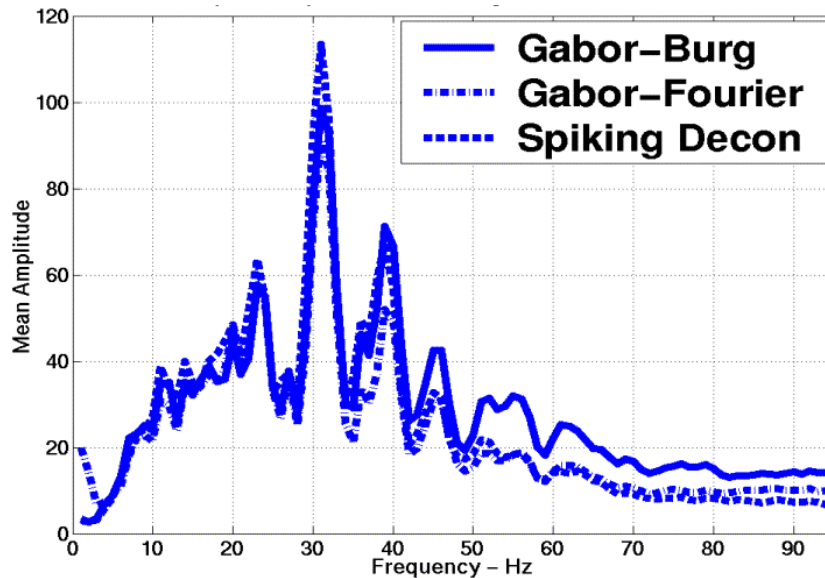


FIG. 13. The Mean amplitude spectra calculated in the time window frame of 0.6-1.3 seconds for the Gabor/ Fourier Gabor/Burg and Wiener spiking sections.

The next step in the processing flow was F-X spatial prediction applied to the data in both cases with the same parameters selected. The type of filter was Wiener Levinson; horizontal window length was 10 samples; time-window length was 500 milliseconds with an overlap of 100 milliseconds. The F-X filter was set between 12 and 100 Hz.

In order to enlarge the bandwidth of the spectra and to increase the resolution of the section the TVSW process was applied to the Wiener spiking section. For the Gabor sections, the deconvolution was run a second time with a minimum-phase deconvolution operator, assuming that the data is closer to a minimum-phase state rather than to zero-phase. However, to be consistent with the zero-phase TVSW method, applied to the Wiener spiking deconvolution, a zero-phase deconvolution was also applied to the Gabor sections. The F-X spectra were again analyzed, and in all three cases. Figures 14, 15 and 16 illustrate the phase spectra after zero-phase deconvolution applied to the Gabor/Fourier and Gabor/Burg sections and the phase spectra of the spiking Wiener section for the same time-window frame (0.6-1.3 seconds).

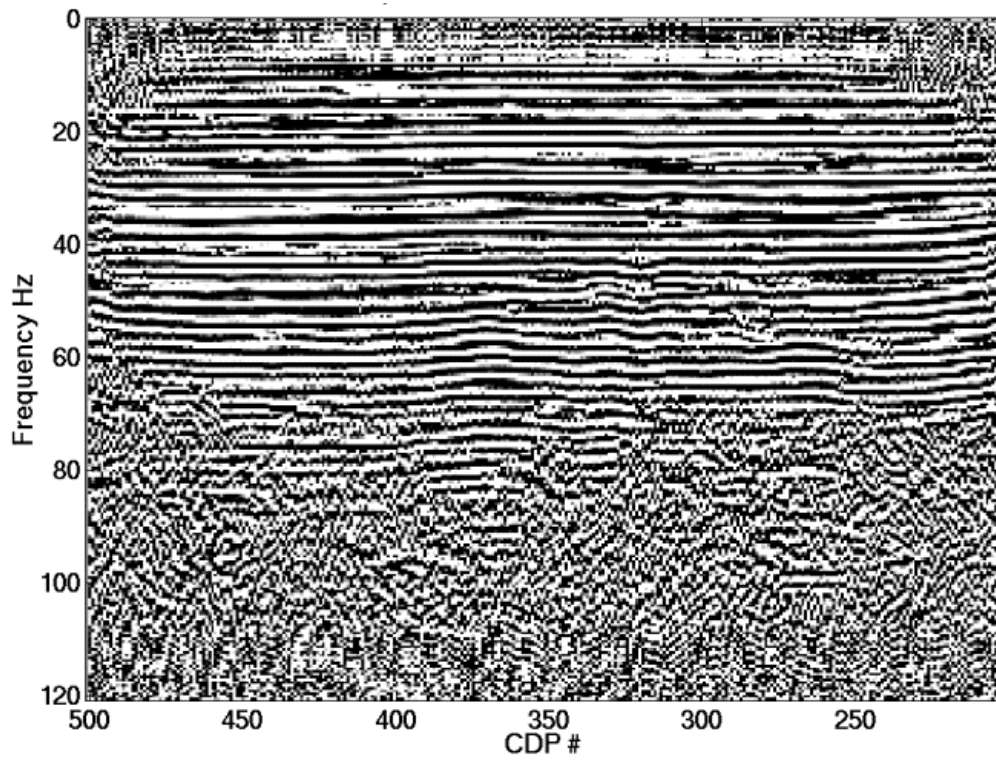


FIG. 14. F-X phase spectrum in the time window 0.6 – 1.3 seconds of the Gabor/Fourier section after zero-phase whitening.

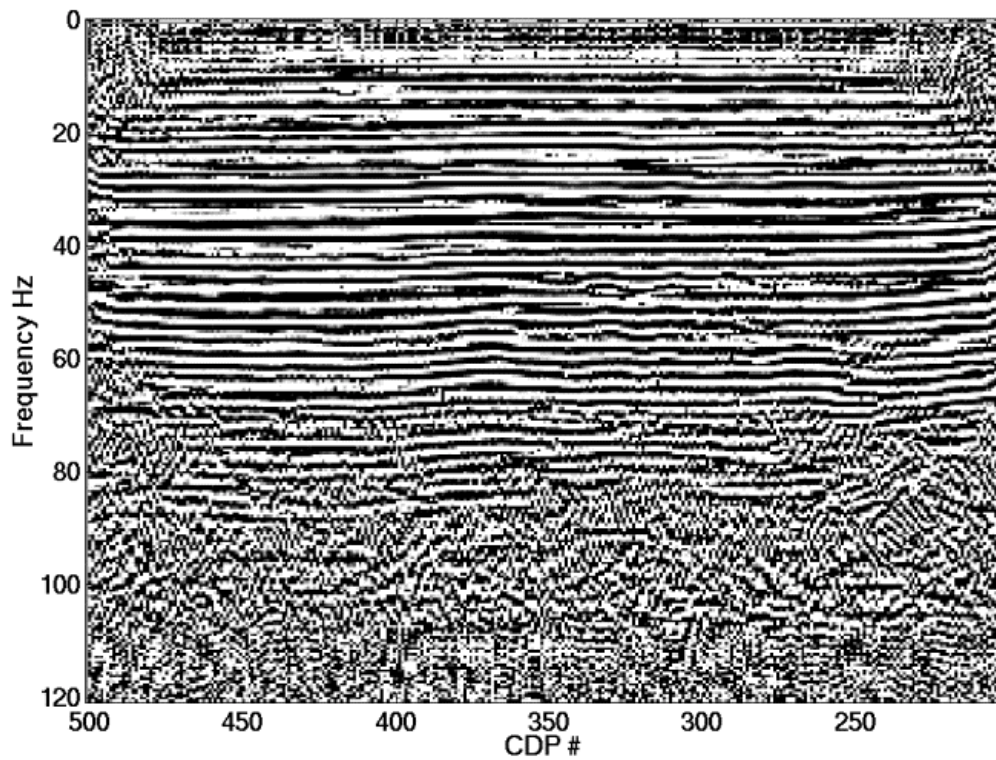


FIG. 15. F-X phase spectrum in the time window 0.6 – 1.3 seconds of the Gabor/Burg section after zero-phase whitening.

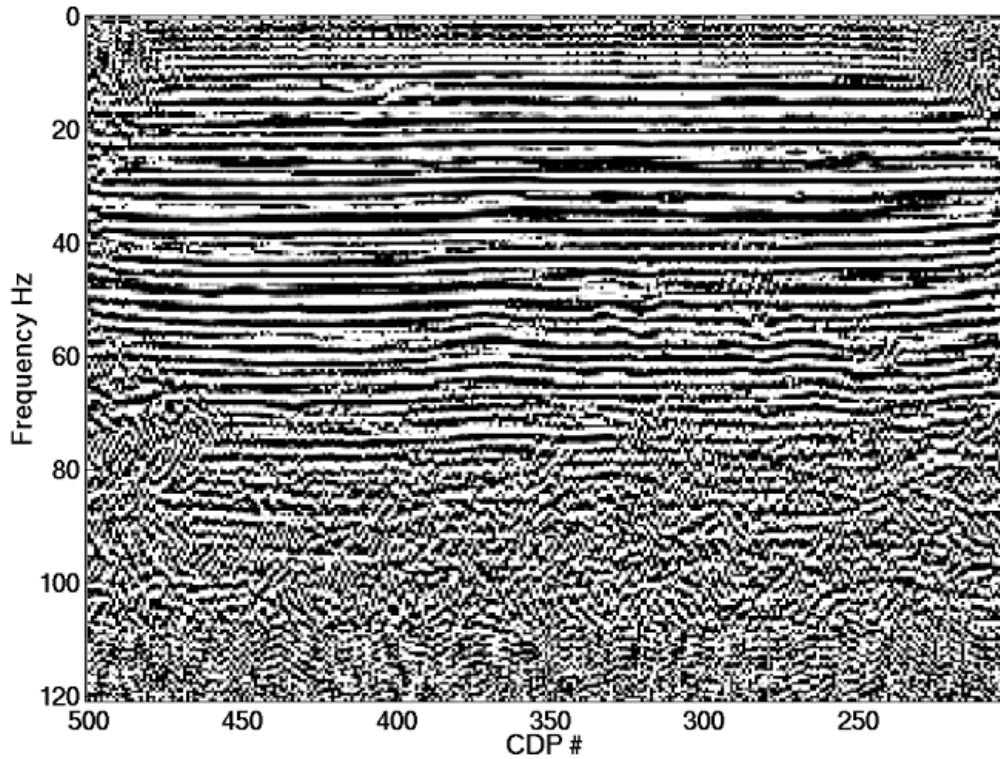


FIG. 16. F-X phase spectrum in the time window 0.6 – 1.3 seconds of the Wiener spiking section after the TVSW.

A band pass filter between 12 and 110 Hz has been applied. The effect of the filter can be observed as a quasi coherence above 100 Hz in all these three pictures and does not indicate signal. In this case, it can be observed that phase coherence indicates signal at more than 85 Hz in the Gabor/Burg section and up to 80 Hz in the Wiener spiking and Gabor/Fourier sections, implying that the signal is better represented in the Gabor/Burg section. The average values for the amplitude spectra were analyzed again after whitening, in all three cases, showing stronger picks toward 80Hz in the Gabor (Fourier/Burg) cases than in the spiking Wiener/TVSW (See Figure 17). The Gabor deconvolution was repeated after stacking with a minimum-phase operator.

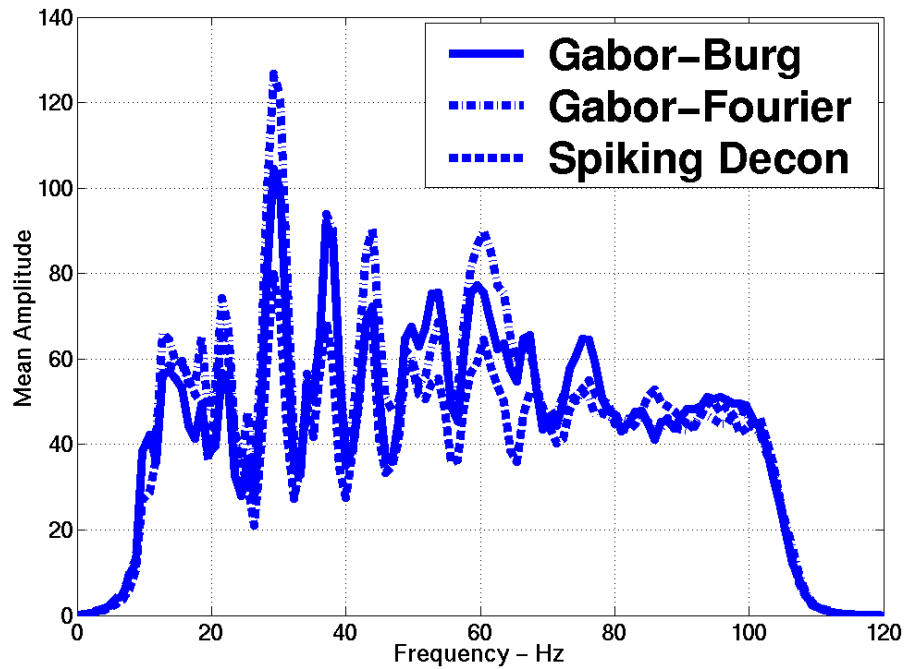


FIG. 17. The mean-amplitude spectra calculated after whitening in the time-window frame of 0.6-1.3 seconds for the Gabor/ Fourier Gabor/Burg and Wiener spiking sections.

The whitened sections (after F-X prediction) are shown in Figures 18 (Gabor/Fourier), 19 (Gabor/Burg), and 20 (Wiener/TVSW). The Glauconitic channels can be observed in all three figures starting from the CDP 350 toward the left of the section. Comparing these sections with the sections before whitening it can be observed that the resolution has been improved and the structural details are easily seen.

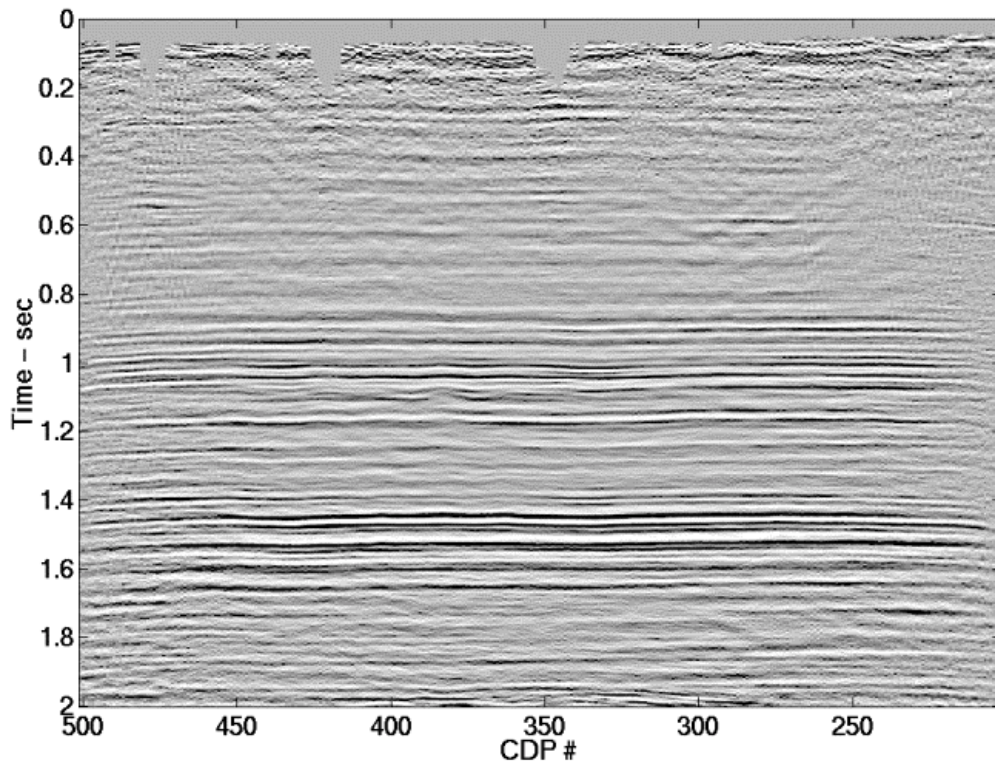


FIG. 18. Gabor/Fourier stack section, minimum-phase, after F-X spatial prediction.

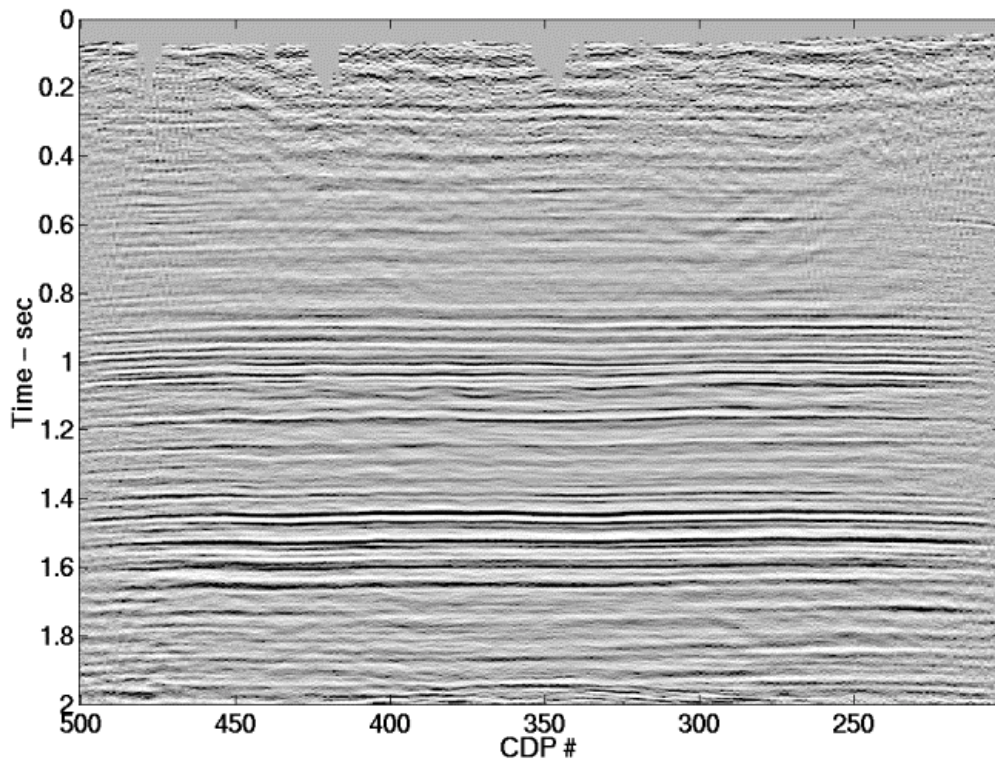


FIG. 19. Gabor/Burg stack section, minimum-phase, after F-X spatial prediction.

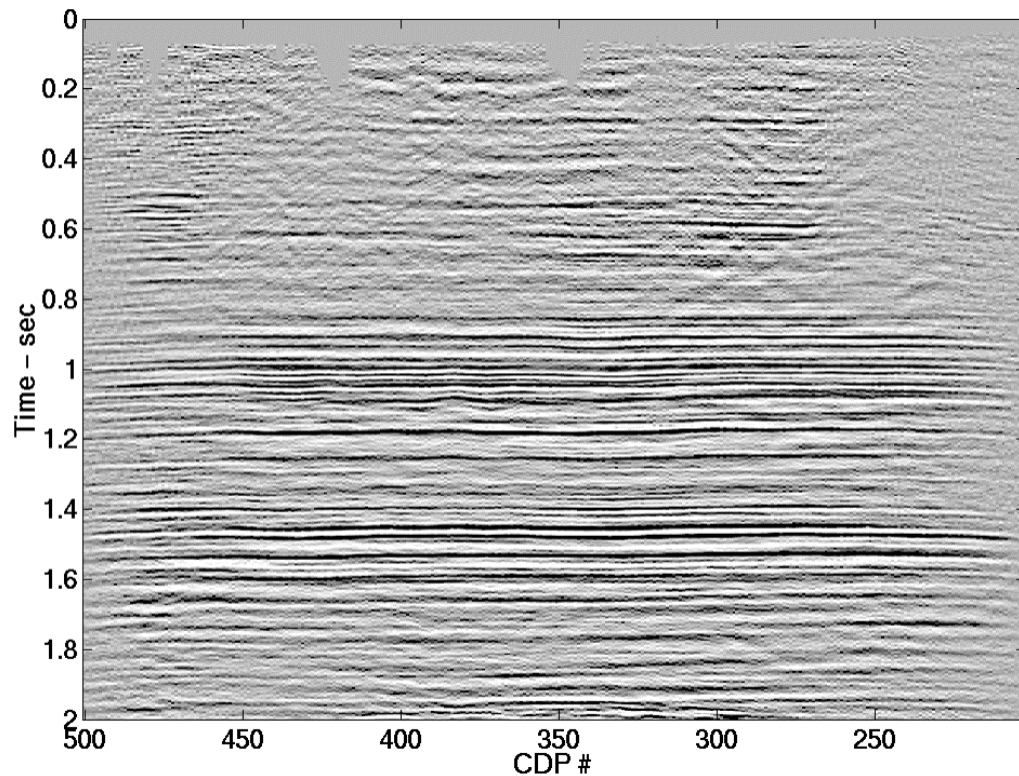


FIG. 20. Wiener stack section, zero-phase, after F-X spatial prediction.

The last step in the processing flows was post stack, phase-shift migration. Again, the same interval velocity file was used in both flows for the phase-shift migration.

The final sections are illustrated in Figures 21 (Gabor/Fourier), 22 (Gabor/Burg), and 23 (Wiener/TVSW). Figure 24 shows in detail the Glauconitic channels, from the Wiener/TVSW section.

The difference between zero-phase and minimum-phase delay state can be better observed on the detailed pictures (Figures 25a, 25b, Gabor/Fourier, and 26a, 26b, Gabor/Burg). In comparison with the zero-phase sections, including also the Wiener/TVSW section (Figure 24), the minimum-phase sections have all the horizons raised to earlier times. This occurs because the zero-phase deconvolution applied after stacking cannot remove the residual wavelet phase effect; while, the minimum-phase sections have less residual phase effect. From this point of view, the events in the minimum-phase sections should be closer to the right position. In addition, two close events on the minimum-phase sections are better delineated and this indicates that the resolution of the minimum-phase sections is better (see Figures 25a/25b and 26a/26b, inside the white oval indicating the Glauconitic channels; or, for example, observe the two horizons at approximately 1180 ms).

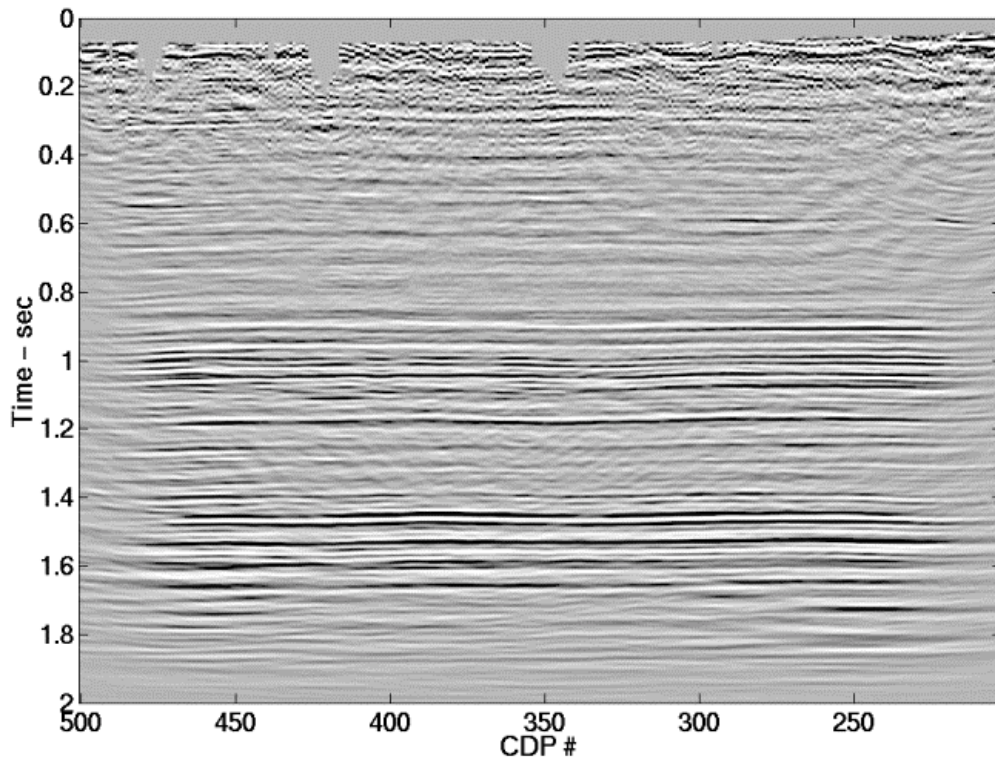


FIG. 21. Migrated section - Gabor/Fourier.

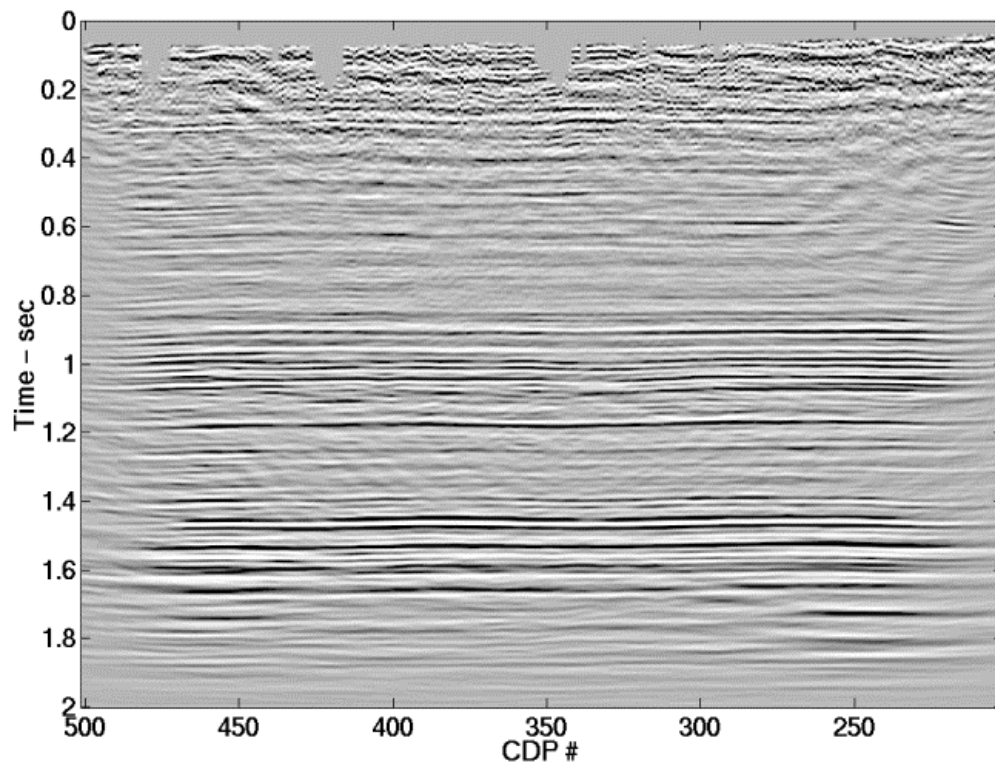


FIG. 22. Migrated section - Gabor/Burg.

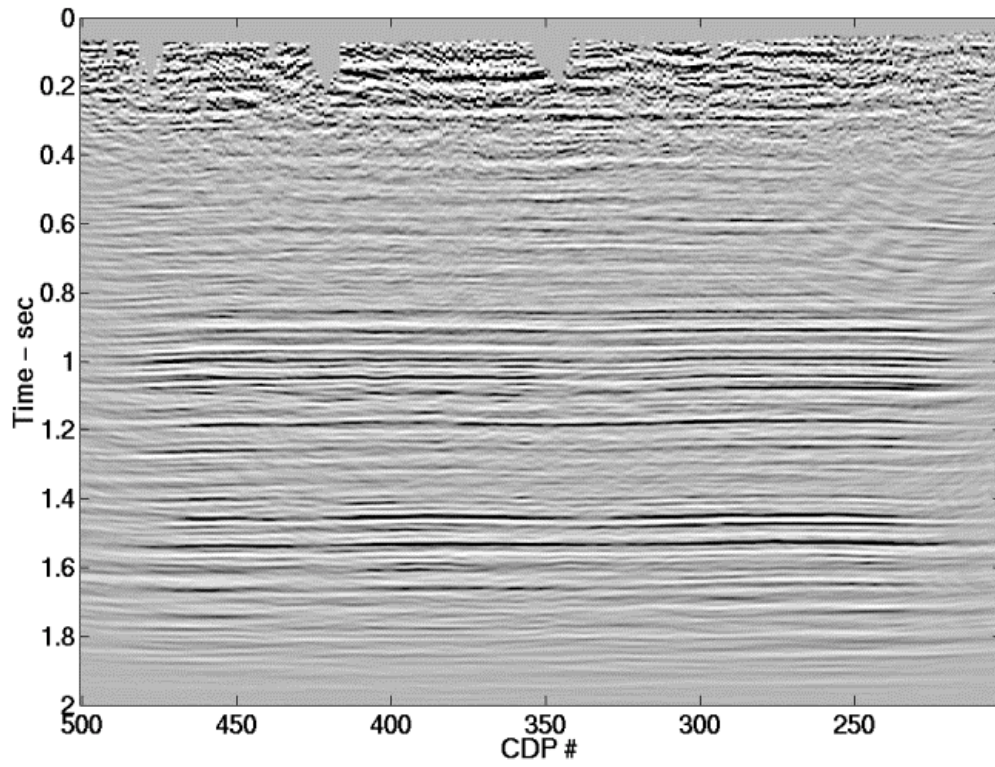


FIG. 23. Migrated section - Wiener/TVSW.

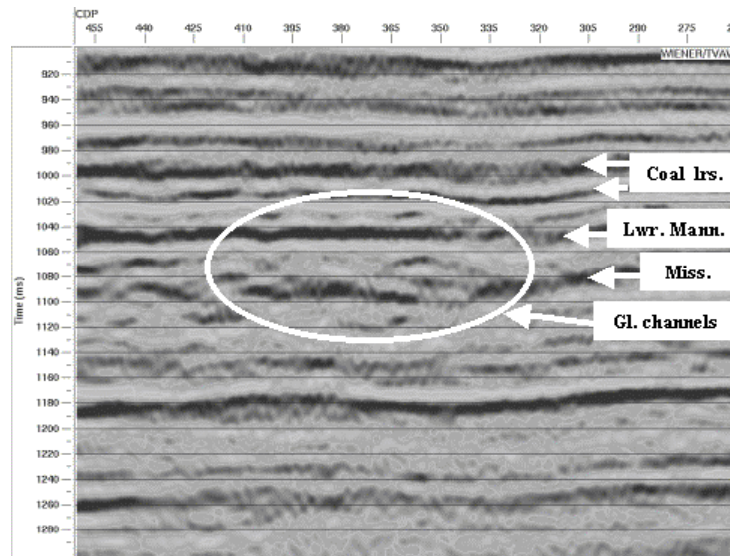


FIG. 24. Migrated section, detail -Wiener/TVSW.

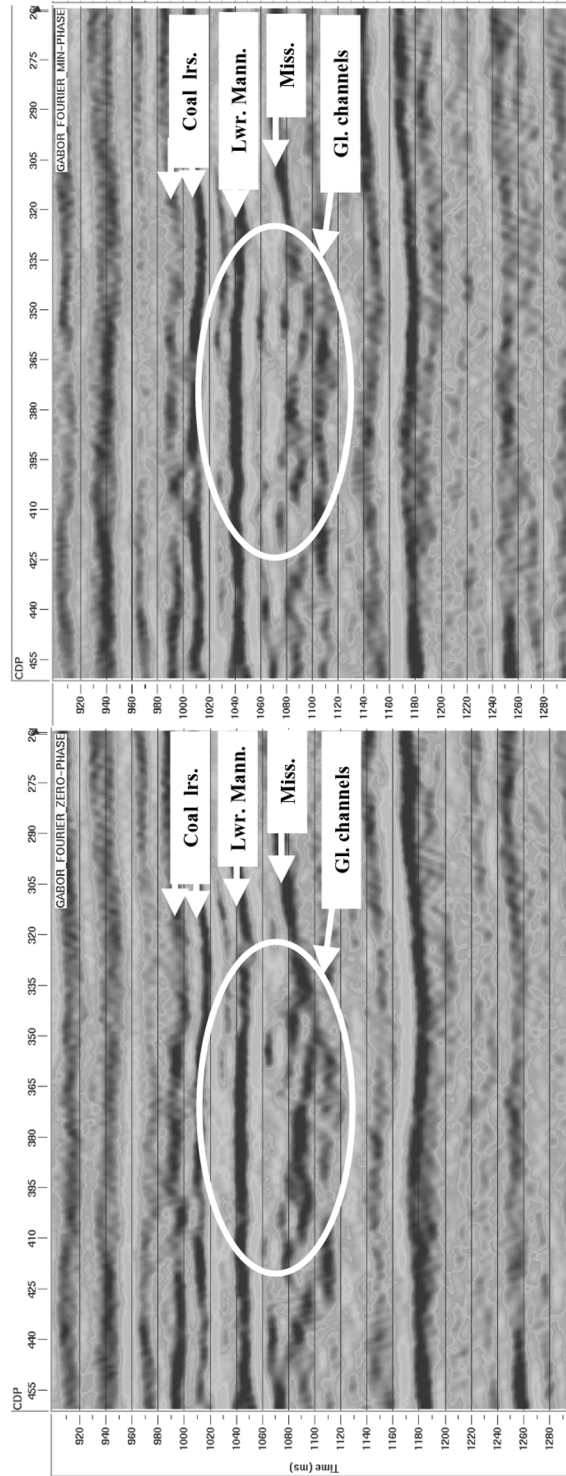


FIG. 25a. Migrated section, detail - Gabor/Fourier – zero-phase.

FIG. 25b. Migrated section, detail- Gabor/Fourier – minimum-phase.

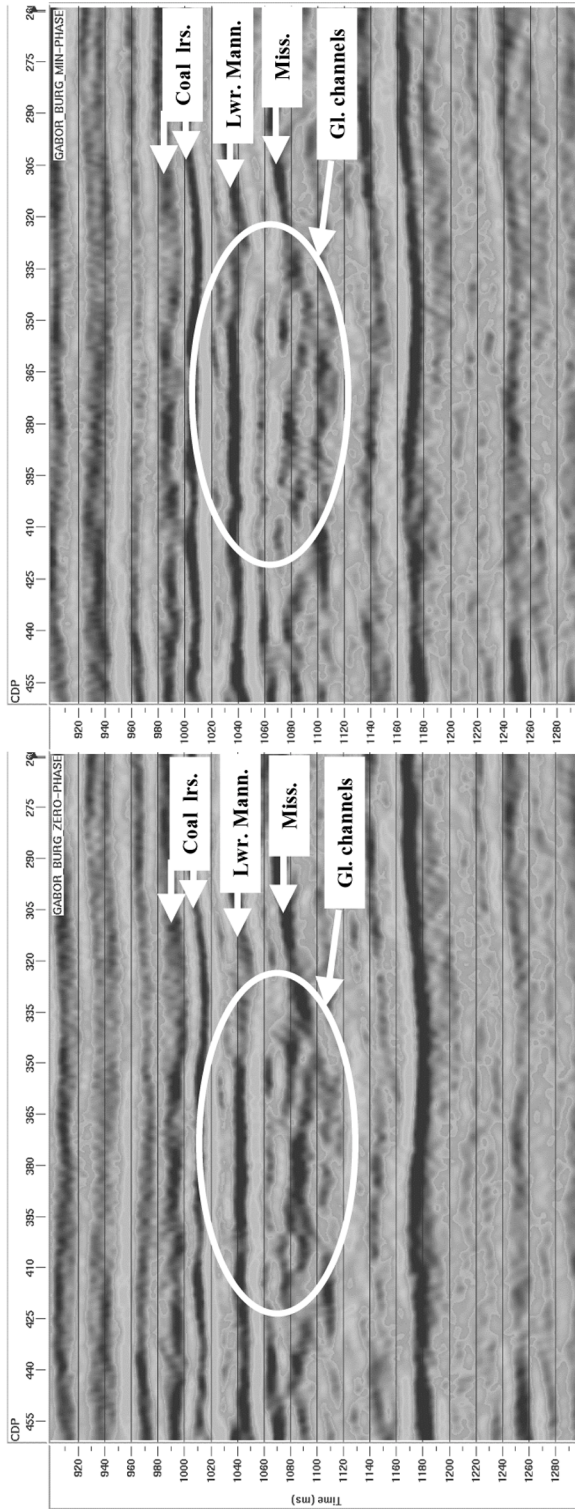


FIG. 26a. Migrated section, detail - Gabor/Burg – zero-phase.

FIG. 26b. Migrated section, detail - Gabor/Burg – minimum phase.

In Figures 27, 28 29 and 30, 31, 32 there are detailed views of two shallow zones (0.1-0.5 and 0.3-0.7 seconds) from the migrated sections of Gabor/Fourier, Gabor/Burg and Wiener deconvolutions. The stationary Wiener deconvolution with a gate designed in the zone of interest (0.7-1.9 seconds), presents a lack of coherence compared with the Gabor method and, of the two methods of the Gabor deconvolution, the Burg spectrum shows superior resolution over the Fourier spectrum. This observation is consistent with the idea that stationary deconvolution can work well within its design gate but not elsewhere. Nonstationary Gabor deconvolution is at least equal to Wiener in the latter's design gate and superior elsewhere.

## **CONCLUSIONS AND FUTURE WORK**

The comparison with the Wiener deconvolution on the Blackfoot data has demonstrated that the nonstationary Gabor method performs very well. Gabor deconvolution estimates the time-varying embedded wavelet and efficiently designs a nonstationary inverse operator to remove it. This inverse operator not only inverts the embedded wavelet as well as Wiener deconvolution can do (in its design window) but also, applies a data dependent Q-filter and a time varying trace balance. Therefore, Gabor deconvolution replaces not only Wiener deconvolution but also exponential gain (or inverse Q-filtering) and AGC. In a future work, Gabor deconvolution will be tested on highly attenuated data, where is expected to offer superior resolution over stationary deconvolution. We will also more closely examine the effects of coherent noise on Gabor deconvolution.

## **ACKNOWLEDGEMENTS**

We would like to thank the sponsors of the CREWES project for their financial support. We also thank Han-Xing Lu from CREWES for useful discussions on processing of seismic data.

## **REFERENCES**

- Claerbout, J.F., 1992, *Earth Soundings analysis - Processing versus inversion*: Blackwell Sc. Public.
- Henley, D.C. and Margrave, G.F., 2001, A ProMax implementation of nonstationary deconvolution: CREWES Research Report, this volume.
- Margrave, G.F., 1999, Seismic signal band estimation by interpretation of f-x spectra: *Geophysics*, **64**, 251-260.
- Margrave, G.F. and Lamoureux, M.P., 2001, Gabor deconvolution, CREWES Research Report, this volume.
- Miller, S.M., Aydemir, E.O., and Margrave, G.F., 1995, Preliminary interpretation of P-P and P-S seismic data from the Blackfoot broad-band survey: CREWES Research Report, 42-1 – 42-17.
- Yilmaz, O., 1987, *Seismic data processing*: Soc. Of Expl. Geophys.

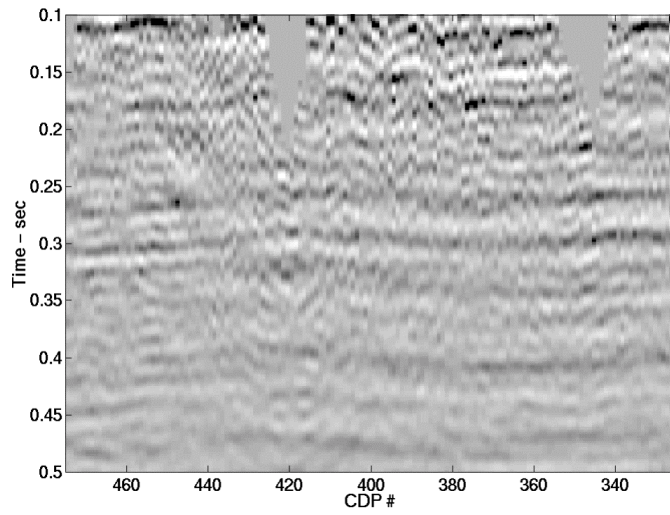


FIG. 27. Final section, detail (0.1-0.5 sec.) – Gabor/Fourier.

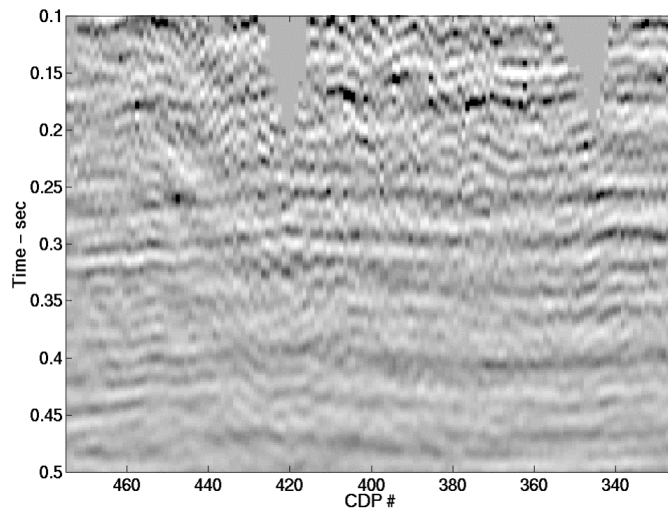


FIG. 28. Final section, detail (0.1-0.5 sec.) – Gabor/Burg.

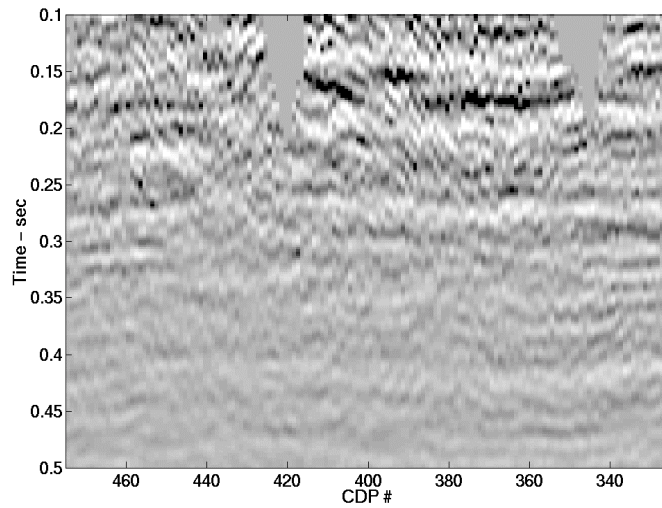


FIG. 29. Final section, detail (0.1-0.5 sec.) - Wiener/TVSW.

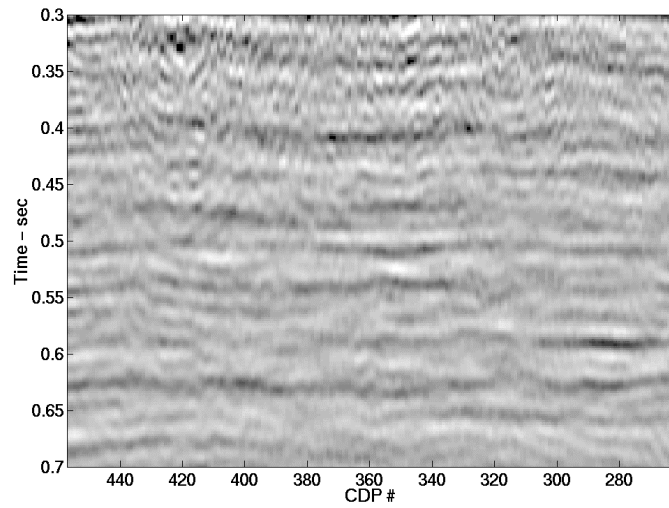


FIG. 30. Final section, detail (0.3-0.7 sec.) - Gabor/Fourier.

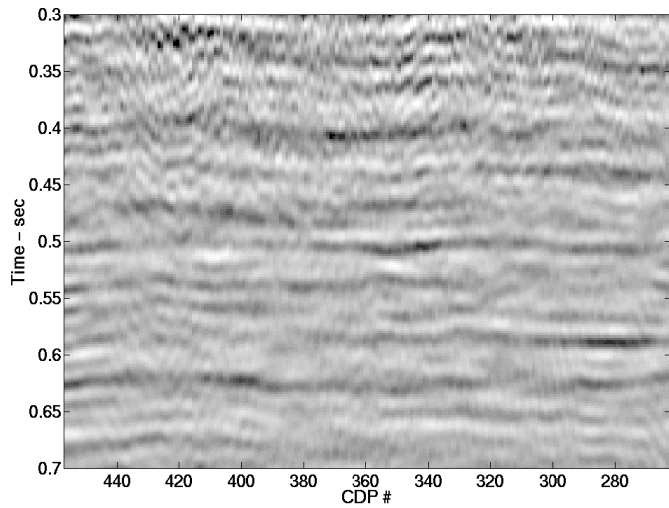


FIG. 31. Final section, detail (0.3-0.7 sec.) - Gabor/Burg.

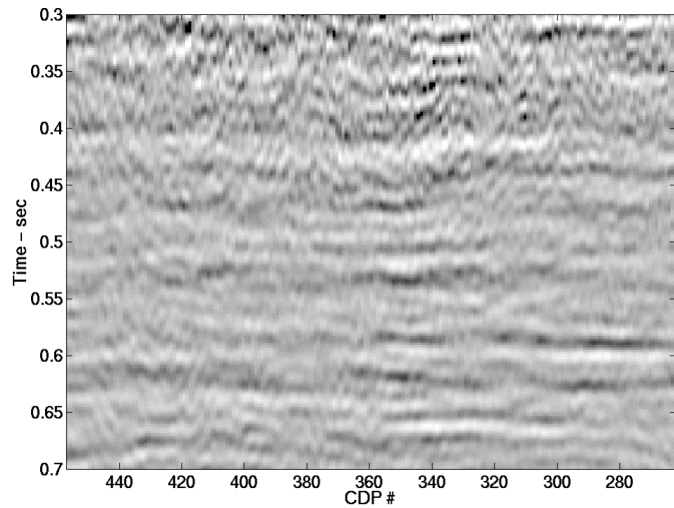


FIG. 32. Final section, detail (0.1-0.5 sec.) - Wiener/TVSW.